THE ASTROPHYSICAL JOURNAL: 212:488–493, 1977 March 1

THE EFFECTS OF WINDS AND CORONAE OF HOT STARS ON THE INFRARED AND RADIO CONTINUA

JOSEPH P. CASSINELLI AND LEE HARTMANN
Washburn Observatory, University of Wisconsin
Received 1976 August 2

ABSTRACT

The theory of the formation of infrared and radio continua is extended to include the effects of steep temperature gradients and coronae. The presence of high-temperature zones in the winds from hot stars has been suggested by recent *Copernicus* satellite observations. We consider models in which the temperature is large only over a small range in radius. The density in the winds of hot stars is high enough for recombination to cool the flow where mechanical energy deposition ceases. Excess radiation at long wavelengths arises in the winds because of the λ^2 dependence of free-free opacity. We find the coronal region causes a broad bump in the infrared continuum at about 20–100 μm with a maximum excess of almost 2 mag. Variations of the distribution of density with height can also cause turnover in the continuous energy distribution; however, only temperature decreases, as occurs in the recombination region, can cause spectral gradients much steeper than the Rayleigh-Jeans gradient.

Subject headings: stars: coronae — stars: early-type — stars: winds

I. INTRODUCTION

The infrared and radio fluxes of hot stars with stellar winds have been discussed by many authors (Gehrz, Hackwell, and Jones 1974; Hackwell, Gehrz, and Smith 1974; Panagia and Felli 1975; Wright and Barlow 1975; Cohen, Kuhi, and Barlow 1975). The excess was interpreted as free-free emission from hot gas in radiative equilibrium. However, recent theoretical and observational work (Hearn 1975; Morton 1976; Lamers and Rogerson 1975; Lamers and Morton 1976) suggests that early-type stars may have high-temperature outer regions or coronae. In this paper we investigate how coronae can affect the long wavelength spectrum and suggest observations to place constraints on possible temperature distributions and flow structure.

We are led to consider the possibility of high-temperature regions in the winds of hot stars because of the recent *Copernicus* satellite observations of O VI in O stars, and because several plausible sources of nonradiative flux have recently been suggested. Snow and Morton (1976), Lamers and Rogerson (1975), and Lamers and Morton (1976) discuss observations of high states of ionization in O stars. Lamers and Morton (1976) have derived a semiempirical model for the O4f star ζ Pup from the ultraviolet P Cygni line profiles. They found that the state of ionization could be explained by an electron temperature of 2×10^5 K, and that it is difficult to produce the O VI ions radiatively because of the sharp reduction of the photospheric continuum flux shortward of the He II ionization edge at 228 Å. Hearn (1975) has explained relatively weak absorption component of the Hα P Cygni line in ζ Ori O9.5 Ia by assuming a very high-temperature region that extends out to 2 stellar radii.

The origin of the mechanical flux required to support the high non–radiative-equilibrium temperatures is uncertain. Solar type convection zones should not exist in these stars. However, other sources of mechanical energy may exist. Aizenman, Hansen, and Ross (1975) have mentioned dissipation of energy by coupling of nonradial modes of oscillation to the unstable radial modes in massive stars. Hearn (1973) argues that small acoustic perturbations in the atmospheres could be amplified by interaction of the sound waves with the radiation field in luminous stars.

Here we will examine observational consequences of various coronae on the infrared and radio flux to provide tests for the existence of coronae. We shall briefly discuss the available observational data relevant to the structure of coronal regions.

II. APPROXIMATE THEORY FOR THE CONTINUOUS SPECTRUM

The basic features of the problem can be understood with a simple treatment of the radiative transfer. We assume that the luminosity at any wavelength is given by thermal emission from the surface at radial optical depth $\tau_\lambda = \frac{1}{3}$. The effective radius is $\tau_\lambda = \frac{1}{3}$ instead of the usual $\tau_\lambda = \frac{2}{3}$ that arises in the Eddington-Barbier relation because extended atmosphere geometry gives added weight to emission from small optical depth; the equivalent uniform disk radius determined from an interferometer occurs at $\tau_\lambda \approx \frac{1}{3}$

(Castor 1974; Cassinelli and Hoffman 1975). In this approximation

$$L_\lambda = 4\pi R_\lambda^2 \pi B_\lambda(\tau_\lambda = \tfrac{1}{3}) = 4\pi^2 R^2 \frac{2c^2 kT(R_\lambda)}{\lambda^4}, \quad (1)$$

where R_λ is the effective radius (at $\tau_\lambda = \frac{1}{3}$), and we have introduced the Rayleigh-Jeans approximation that is appropriate for our problem. Given the density distribution $\rho(r)$ and the temperature distribution $T(r)$, the free-free opacity can be integrated to find the value of $r = R_\lambda$ where $\tau_\lambda = \frac{1}{3}$. Since $k_\lambda \propto \rho^2 T^{-3/2} \lambda^2$, the effective radius will increase with wavelength and so produce an excess of radiation above the Rayleigh-Jeans tail at long wavelengths.

At the simplest level of approximation, consider a model in which $\rho \propto r^{-n}$ and $T \propto r^{-m}$. Then

$$R_\lambda \propto \lambda^{-2/(-2n+3m/2+1)}. \quad (2)$$

Combining (1) and (2), we have

$$\lambda L_\lambda \propto \lambda^s,$$

where

$$s = \frac{6n - \frac{5}{2}m - 7}{-2n + \frac{3}{2}m + 1}.$$

As n approaches infinity, $R_\lambda \rightarrow$ constant and $s = -3$, which is the Rayleigh-Jeans distribution for plane-parallel atmospheres. If the flow is steady, then conservation of mass requires that a large value of n correspond to a large velocity gradient ($v \propto \rho^{-1} r^{-2} \propto r^{-2n}$). In regions of constant flow speed $n = 2$, and we find $s = -5/3$ independent of the temperature gradient index m. This corresponds to the most important case treated by Panagia and Felli (1975) and Wright and Barlow (1975).

For convenience we give a short list of s for various n and m values in Table 1. For $n = 2$, temperature gradients do not affect the spectrum. This is also the case for n approaching infinity unless m is comparable to n. For $n = 3$, which corresponds to a linear velocity gradient, there *is* a dependence on the temperature gradient. The amount of the excess of radiation above the Rayleigh-Jeans tail increases if T increases outward ($m < 0$) and decreases if T decreases outward ($m > 0$).

A flux gradient steeper than $s = -3$ does not occur unless there is a temperature decrease. This corresponds to a decreasing excess of long wavelength radiation and is a phenomenon that does not occur if only variations in velocity or density gradients are considered.

We note that this simple theory cannot be used for $|m| \gg 1$ or $m \ll -1$. Such choices lead to divergences in the opacity at large r, and so in any realistic situation one must introduce a cutoff or boundary. Keeping this in mind, this simple approximation gives the qualitative dependence of the infrared flux on temperature and density gradients.

III. CORONAL MODELS

In another paper (Hartmann and Cassinelli 1977) we consider the fluxes from radiative equilibrium atmospheres; here we are concerned with coronal effects.

To isolate the effect of high-temperature zones we shall consider several temperature distributions but only one velocity distribution. We have chosen a velocity law derived in part by the Lamers and Morton (1976) analysis of ζ Pup. The density distribution follows, given a mass loss rate; Lamers and Morton derived a rate of $7.2 \times 10^{-6}\ M_\odot\ \mathrm{yr}^{-1}$. The photosphere of our model is assumed to be geometrically thin, and the relative density follows a simple scale height law. In the flow regime we assume the velocity increases linearly out to 1.5 stellar radii (where $v = 25\%$ of the terminal speed) and follows the Lamers-Morton expression $v^2 = v_0^2 + v_1^2(1 - R_*/r)$ beyond that, approaching 2800 km s^{-1} asymptotically at large r.

For our temperature distribution we assume $T^4 \propto \tau + \frac{2}{3}$ in the photosphere. In the flow regime we assume there is a transition region where the temperature rises linearly to the coronal value T_c, a plateau at T_c, and a recombination region in which the temperature decreases linearly to a low value appropriate for radiative equilibrium, T_{RE}. This distribution is shown in Figure 1. The drop in temperature in the recombination region does not occur in the solar corona. However, such a drop is plausible because the densities in Of winds are high, of order 10^{11} cm^{-3}, and so radiative cooling is effective, and the temperature should decrease rapidly where mechanical energy deposition is not large (Hearn 1975).

For our calculations we considered the three temperature distributions displayed in Figure 1, two values for the coronal temperature T_c (2×10^5 and 2×10^6 K), two values for the mass loss rate (7.2×10^{-6} and $1.44 \times 10^{-5}\ M_\odot\ \mathrm{yr}^{-1}$), and assumed a hydrogen to helium number ratio of 10. We computed the emergent fluxes using the variable Eddington factor method (Cassinelli and Hartmann 1975). The results for λL_λ are given in Table 2, and two cases are

TABLE 1

SPECTRAL INDEX DEPENDENCE ON TEMPERATURE AND DENSITY GRADIENTS

n.....	2	∞	3	3	3	3	3/2
m.....	any	any	0	−1	−3	+3	0
s.....	−1.67	−3	−2.2	−2.08	−1.95	−7	−1

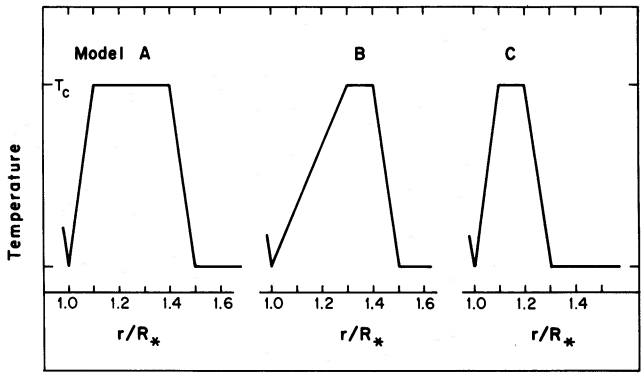

FIG. 1.—The run of temperature versus radius, in stellar radii, for the three models considered. T_c is the coronal temperature.

displayed in Figure 2. The coronal zone gives rise to a broad continuum "bump" at ~ 10 μm to 100 μm as is seen in Figure 2. Also shown is the distribution of a model with no corona. The maximum infrared excess caused by the corona is about 1.8 mag for the corona with $T_c = 2 \times 10^6$ and about 1.1 mag for the corona with $T_c = 2 \times 10^5$. The spectral slope at the long wavelength side of the bump is ~ -4.0, larger than the Rayleigh-Jeans slope of $s = -3.0$. The sudden onset of decreasing excesses such as this have been seen in the infrared distribution of several very young stars (John Warner, private communication), and perhaps steep temperature declines are the cause.

The lower part of Figure 2 shows the effect of doubling the mass loss rate. The theory of § II may be used to show

$$\dot{M} \propto \lambda^2 L_\lambda^{3/4} v_\infty .$$

Thus the monochromatic luminosity varies with mass loss rate as $M^{4/3}$. This is in good agreement with our numerical results. The spectral gradient from the infrared to the radio extrapolates with a slope of about $s = -1.58$, so we have not shown the longer wavelengths in our figure.

To check these results we may use the simple theory of § II. Given a density and temperature distribution, we can numerically integrate the free-free opacity to find R_λ, and use equation (1) to find L_λ. This approximate calculation is compared to the exact result in Figure 3. The comparison shows reasonable agreement if the coronal "bump" of the approximate theory is "smeared out." It is not hard to see that this should be so. In reality, contributions to emergent flux come from many layers, not just $\tau_\lambda = \frac{1}{3}$, and if conditions are rapidly varying through these layers it certainly will not be a good approximation to ignore all but $\tau_\lambda = \frac{1}{3}$. We can estimate the size of this by using a two-point Gaussian quadrature in τ_λ for the flux, which simply means that we regard L_λ as now

TABLE 2

MONOCHROMATIC LUMINOSITIES OF STAR MODELS

Model	A	A	B	C	C	No Corona
T_c (K)	2×10^6	2×10^5	2×10^6	2×10^6	2×10^6	...
dM/dt ($M_\odot$ yr^{-1})	7.2×10^{-6}	7.2×10^{-6}	7.2×10^{-6}	7.2×10^{-6}	1.44×10^{-5}	7.2×10^{-6}
			log λL_λ (ergs s^{-1})			
5053 Å	38.036	38.036	38.036	38.036	37.984	38.037
8210 Å	37.480	37.482	37.481	37.480	37.441	37.481
1.000 μm	37.244	37.247	37.246	37.245	37.211	37.246
1.500 μm	36.753	36.759	36.756	36.754	36.736	36.756
3.000 μm	35.965	35.939	35.959	35.965	36.120	35.910
3.750 μm	35.727	35.690	35.718	35.727	35.936	35.640
5.000 μm	35.445	35.386	35.429	35.445	35.720	35.297
7.500 μm	35.096	34.993	35.066	35.096	35.429	34.824
10.00 μm	34.879	34.734	34.833	34.876	...	34.499
15.00 μm	34.590	34.380	34.515	34.576	34.841	34.061
20.00 μm	34.381	34.124	34.284	34.345	...	33.756
30.00 μm	34.060	33.743	33.938	33.954	33.858	33.337
33.33 μm	33.970	33.637	33.843	33.833	...	33.230
37.50 μm	33.866	33.515	33.734	33.684	33.450	33.112
50.00 μm	33.585	33.194	33.447	33.254	33.098	32.828
75.00 μm	33.099	32.675	32.961	32.539	32.799	32.447
0.150 mm	31.933	31.839	31.900	31.847	32.173	31.835
0.300 mm	31.288	31.288	31.292	31.310	31.648	31.295
0.375 mm	31.119	31.119	31.115	31.114	31.477	31.128

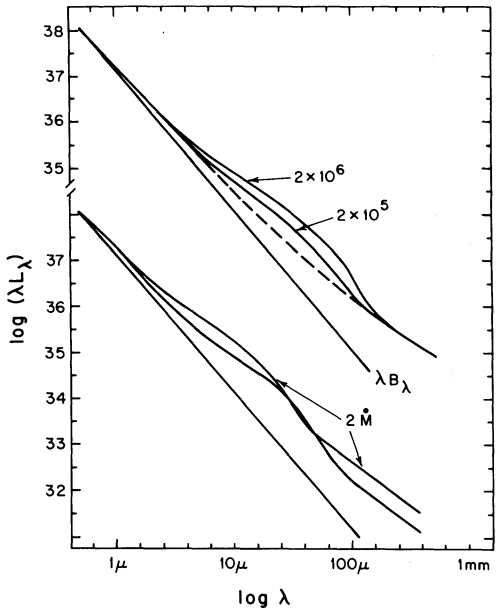

FIG. 2.—The continuous energy distribution in the IR. The upper portion shows the dependence of the emergent continuum on the assumed value for the coronal temperature, T_c. These curves are labeled with the value of T_c and are compared with the Planck distribution and with a model having no coronal zone, plotted with a dashed line. The coronal models correspond to temperature model A with a mass loss rate $7.2 \times 10^{-6}\ M_\odot\ \mathrm{yr}^{-1}$. The lower curve shows the dependence of the continuum on the assumed value of the mass loss rate, given a temperature structure. These curves are for temperature model C with $T_c = 2 \times 10^6$ K and mass loss rates 7.2×10^{-6} and $1.44 \times 10^{-5}\ M_\odot\ \mathrm{yr}^{-1}$; the higher mass loss rate is labeled as $2\dot{M}$. The run of the Planck function is repeated for comparison.

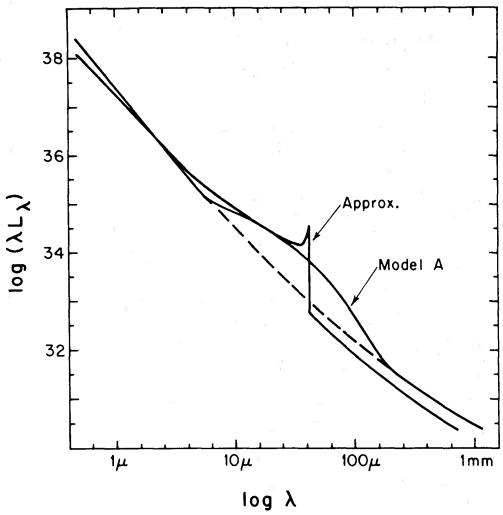

FIG. 3.—Monochromatic continuous energy distributions for the approximate theory of § I compared with the results of the accurate numerical calculations. The curves correspond to temperature model A with mass loss rate of $7.2 \times 10^{-6}\ M_\odot\ \mathrm{yr}^{-1}$, $T_c = 2 \times 10^6$ K. The dashed line is the emergent continuum in absence of a coronal temperature rise.

coming from two depths instead of one. This correction indicates $\Delta \log \lambda \approx 0.4$ for smearing.

Another factor which causes "smearing" is the electron scattering opacity, which dominates at short wavelengths and at high temperatures. Now the opacity is proportional to λ^t, where $t < 2$; this smears because a single layer at r has a wider range of λ for which $\tau_\lambda \approx \frac{1}{3}$. In addition, the long thermalization length caused by adding electron scattering enhances the contributions of deeper layers to the flux. The effects of electron scattering in extended atmospheres have been discussed by Castor (1974). The emergent flux is given approximately by

$$H_\lambda = \frac{\epsilon_\lambda^{1/2}}{1 + \epsilon_\lambda^{1/2}} B_\lambda\left(\tau_\lambda = \frac{1}{(3\epsilon_\lambda)^{1/2}}\right),$$

where ϵ_λ is the ratio of absorptive to total opacity. The ratio ϵ_λ tends to increase with wavelength, causing the factor in front of the Planck function to increase. This tends to cause an infrared excess. The Planck function itself is to be evaluated at unit thermalization depth. In the corona B_λ is large but ϵ is negligibly small, thus at the wavelength at which one should "see" the corona, according to the simple theory one actually sees scattered radiation that was formed mostly below the corona.

Figure 4 shows the effect of changing the model parameters. We should expect the bump to shift to shorter wavelengths if we increase the optical depth of the outer radiative equilibrium region. This may be done by placing the corona deeper in the atmosphere or by increasing the mass loss rate. In Figure 4

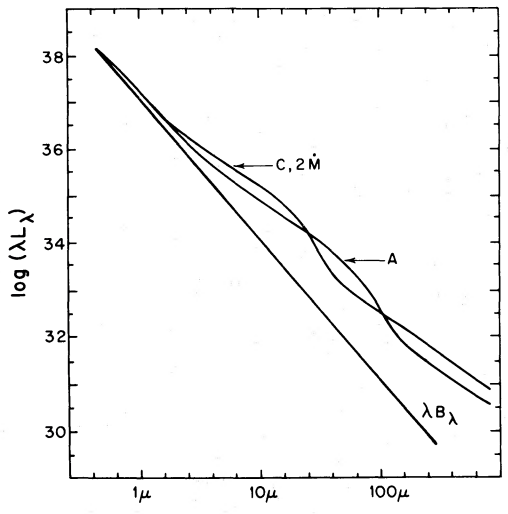

FIG. 4.—The continuous energy distribution for two very different models. The curve labeled A is the same as that shown in Fig. 3. The curve labeled C, $2\dot{M}$ shows the effect of using a model with a recombination region deep in the atmosphere and with a large mass loss rate of $1.44 \times 10^{-5}\ M_\odot\ \mathrm{yr}^{-1}$. The bump is shifted to shorter wavelengths. Both models have $T_c = 2 \times 10^6$ K. Also shown is the Planck function.

we show a model in which the corona is concentrated near the base of the flow (model C) and has a large mass loss rate. This was done to see if excesses in the near infrared could be caused by high-temperature winds. The simple theory of § II leads to such a prediction, but it is not supported by the detailed numerical calculations. The extreme model shown in Figure 4 does not have a significant excess in the near-IR because electron scattering dominates the short wavelength opacity, and we see light originating at unit thermalization depth.

We have also considered the effect of placing the temperature rise in the plane-parallel photospheric region where the density is high enough for free-free opacity at a few micrometers to be comparable to electron scattering opacity. This means that the temperature rises at $\tau_{es} \approx 0.3$. This temperature rise does lead to an excess in the near-infrared. Such a temperature structure can probably be ruled out for the Of stars because they have small excesses at 1 μm, and the visible spectra show photospheric lines of O stars. However, the temperature structure may be relevant to Wolf-Rayet stars which show a strong near-IR excess and have essentially only emission lines in the spectrum. Coronal regions in Wolf-Rayet atmospheres are discussed further by Hartmann and Cassinelli (1977).

The flow models for which we have carried out our radiative transfer calculations have density gradient $n = 3$ in the region where we are permitting coronal temperatures. We are therefore emphasizing the effect of the temperature gradients because if $n = 2$ or $n = \infty$, the temperature dependence of the emergent continuum is negligible, as was discussed in § II. Certainly one would not expect the temperature and density changes to be completely independent. This can be seen from the momentum equation for steady flow (cf. Cassinelli and Hartmann 1975). Using appropriate values for ζ Pup, $M \sim 60\,M_\odot$, $r_* \sim 10^{12}$ cm, we get

$$\frac{d\ln v}{d\ln r} = \frac{2 - d\ln T/d\ln r - (10^8\ \mathrm{K}/T)(1-\Gamma)}{v^2/RT - 1}.$$

Since the temperature variation will undoubtedly affect the radiation pressure factor Γ in a complicated way, it is not clear how the density and velocity will vary with T.

The one peculiar behavior of long wavelength continuum which we have found to be strong evidence for a high-temperature zone is a spectral slope steeper than $s = -3$. This is caused by the recombination region. In the constant-temperature models treated by Hartmann and Cassinelli (1977), the continuum may have abrupt changes in slope but nowhere is the slope steeper than $|s| = 3$.

IV. DISCUSSION OF OBSERVATIONAL DATA

We have shown that high-temperature zones that occur in regions of the atmosphere where there is a linear velocity increase will cause a broad bump in the long wavelength excess. We have assumed that the high-temperature zones are small in radial extent because recombination processes should lead to effective cooling where the mechanical deposition weakens. There is also a good observational reason for expecting this to be the case. An upper limit to the X-ray flux from ζ Pup in the wavelength band 0.20–0.284 keV has been determined by Mewe *et al.* (1975) from ANS satellite observations. The limit of $L_\lambda < 4.6 \times 10^{32}$ ergs s^{-1} requires the high-temperature regions to be limited in spatial extent, as discussed by Lamers and Morton (1976).

In the spectral regions of interest to us here, the longer the wavelength, the larger the apparent radius of the star. At radio wavelengths one should see the outer regions of the flow where the wind has attained terminal speed, and the flux should be nearly independent of the temperature of the gas. The radio flux should therefore be of greatest value in determining mass loss rates. Assuming a distance of 450 pc for ζ Pup and using the mass loss rate of $7.2 \times 10^{-6}\,M_\odot$ yr^{-1}, the flux at 3 cm should be 4 mJy and therefore within the limit of detection. Fluxes of this order have been detected in γ^2 Vel and P Cyg, and respective mass loss rates of $1.5 \times 10^{-5}\,M_\odot$ yr^{-1} and $2 \times 10^{-6}\,M_\odot$ yr^{-1} have been determined (Wright and Barlow 1975; Seaquist 1976; Thorne 1976).

At radio wavelengths one should not detect the coronal regions directly. For this, infrared observations are more appropriate. On the other hand, mass loss rates determined from infrared observations must be considered with care, because at these wavelengths one is probably seeing regions of the atmosphere where the wind has not yet attained terminal

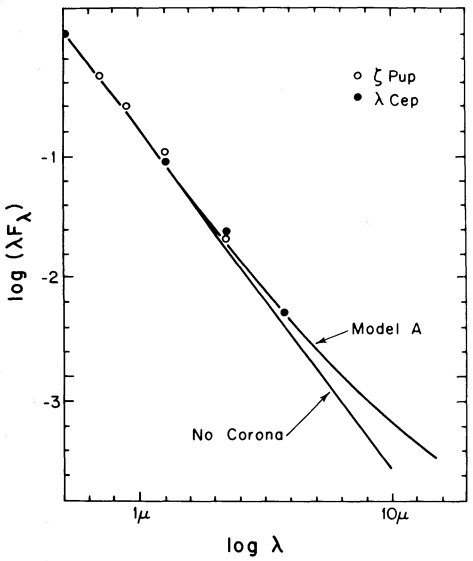

FIG. 5.—Observational data for ζ Pup (O4f) and λ Cep (O6f) in the near-IR compared with the results of coronal model A with $T_c = 2 \times 10^6$ K and mass loss rate $7.2 \times 10^{-6}\,M_\odot$ yr^{-1} and with the continuum distribution for a model with no coronal zone. All curves and data were normalized at 5000 Å.

value, and high-temperature zones may lead to large excesses. These points are discussed in greater detail by Hartmann and Cassinelli (1977).

There are very few data available for the infrared flux of Of stars. In Figure 5 we show the observations from Johnson *et al.* (1966) for ζ Pup O4f and λ Cep O4f. We have estimated the interstellar reddening from OAO-2 data, correcting the flux distribution for the characteristic interstellar bump at 2200 Å, as is discussed by Holm and Cassinelli (1977). For ζ Pup we get $E_{B-V} = 0.04$ $(+0.02, -0.01)$ and for λ Cep we get $E_{B-V} = 0.60 \pm 0.04$. Also shown in Figure 5 are data from model A, $T_c = 2 \times 10^6$, and the model results with no corona. Thus even at 10–20 μm we can see some effects of coronal regions. The maximum excess for model A occurs at 36 μm. For ζ Pup the flux at 36 μm should be about 4 Jy. This is within current detection limits (Harper 1976).

This work was begun while J. P. C. was a visiting scientist at the Astronomical Institute in Utrecht. He wishes to thank Dr. de Jager for his hospitality and Dr. Hearn and Dr. Lamers for many thought-provoking discussions. We are also indebted to Dr. Hearn for suggestions and comments on the manuscript. This work was supported in part by National Science Foundation grant MPS 74-01489.

REFERENCES

Aizenman, M. L., Hansen, C. J., and Ross, R. R. 1975, *Ap. J.*, **201**, 387.
Cassinelli, J. P., and Hartmann, L. 1975, *Ap. J.*, **202**, 718.
Cassinelli, J. P., and Hoffman, C. 1975, *M.N.R.A.S.*, **173**, 789.
Castor, J. I. 1974, *Ap. J.*, **189**, 273.
Cohen, M., Barlow, M. J., and Kuhi, L. V. 1975, *Astr. Ap.*, **40**, 291.
Gehrz, R. D., Hackwell, J. A., and Jones, T. W. 1974, *Astr. Ap.*, **20**, 333.
Hackwell, J. A., Gehrz, R. D., and Smith, J. R. 1974, *Ap. J.*, **192**, 383.
Harper, D. A. 1976, personal communication.
Hartmann, L., and Cassinelli, J. P. 1977, *Ap. J.*, in press.
Hearn, A. G. 1973, *Astr. Ap.*, **23**, 97.
———. 1975, *Astr. Ap.*, **40**, 355.
Holm, A. V., and Cassinelli, J. P. 1977, *Ap. J.*, **211**, 432.
Johnson, H. L., Mitchell, R. I., Iriarte, B., and Wiśniewski, W. Z. 1966, *Comm. Lunar Planet. Lab.*, **4**, 99, No. 63.
Lamers, H. J. G. L. M., and Morton, D. C. 1976, *Ap. J. Suppl.*, **32**, 715.
Lamers, H. J. G. L. M., and Rogerson, J. B. 1975, *Nature*, **256**, 190.
Mewe, R., Heise, J., Gronenschild, E. H. B. M., Brinkman, A. C., Schrijver, J., and den Boggende, A. J. F. 1975, *Ap. J. (Letters)*, **202**, L67.
Morton, D. C. 1976, *Ap. J.*, **203**, 386.
Panagia, N., and Felli, M. 1975, *Astr. Ap.*, **39**, 1.
Seaquist, E. R. 1976, *Ap. J. (Letters)*, **203**, L35.
Snow, T. P., and Morton, D. C. 1976, *Ap. J. Suppl.*, **32**, 429.
Thorne, K. S. 1976, Orange-Aid Preprint, No. 421.
Wright, A. P., and Barlow, M. J. 1975, *M.N.R.A.S.*, **170**, 41.

JOSEPH P. CASSINELLI: Department of Astronomy, Sterling Hall, University of Wisconsin, Madison, WI 53706

LEE HARTMANN: Harvard College Observatory, Center for Astrophysics, 60 Garden Street, Cambridge, MA 02138